Correlation between negative magnetoresistance effect and magnon excitations in single-crystalline CuCr1.6V0.4Se4

Ewa Malicka, Tadeusz Groń, Danuta Skrzypek, Andrzej W. Pacyna, Dariusz Badurski, Alicja Waśkowska, Slawomir Mazur, Rafal Sitko

Correlation between negative magnetoresistance effect and magnon excitations in single-crystalline CuCr1.6V0.4Se4

Journal:	*Philosophical Magazine & Philosophical Magazine Letters*
Manuscript ID:	TPHM-09-Jul-0306
Journal Selection:	Philosophical Magazine
Date Submitted by the Author:	20-Jul-2009
Complete List of Authors:	Malicka, Ewa; University of Silesia, Institute of Chemistry Groń, Tadeusz; University of Silesia, Institute of Physics Skrzypek, Danuta; University of Silesia, Institute of Physics Pacyna, Andrzej; Polish Academy of Sciences, The Henryk Niewodniczański Institute of Nuclear Physics Badurski, Dariusz; Polish Academy of Sciences, Institute of Low Temperatures and Structure Research Waśkowska, Alicja; Polish Academy of Sciences, Institute of Low Temperatures and Structure Research Mazur, Sławomir; University of Silesia, Institute of Physics Sitko, Rafał; University of Silesia, Institute of Chemistry
Keywords:	electron paramagnetic resonance, magnetoresistance, spinels, thermoelectric power
Keywords (user supplied):	magnetoresistance, spin waves, thermoelectric effects

Correlation between negative magnetoresistance effect and magnon excitations in single-crystalline $CuCr_{1.6}V_{0.4}Se_4$

E. Malicka,[1] T. Groń,[2] D. Skrzypek,[2] A.W. Pacyna,[3] D. Badurski,[4]

A. Waśkowska,[4] S. Mazur,[2] and R. Sitko[1]

[1]*University of Silesia, Institute of Chemistry, ul. Szkolna 9, 40-006 Katowice, Poland*

[2]*University of Silesia, Institute of Physics, ul. Uniwersytecka 4, 40-007 Katowice, Poland*

[3]*The Henryk Niewodniczański Institute of Nuclear Physics, Polish Academy of Sciences, ul. Radzikowskiego 152, 31-342 Kraków, Poland*

[4]*Institute of Low Temperature and Structure Research, Polish Academy of Sciences, ul. Okólna 2, 50-950 Wrocław, Poland*

The structural, electrical and magnetic measurements as well as the electron spin resonance (ESR) spectra were used to characterize the single-crystalline $CuCr_{1.6}V_{0.4}Se_4$ spinel and to study a correlation between negative magnetoresistance effect and magnon excitations. The ferromagnetic order below the Curie temperature $T_C \approx$ 193 K, a *p*-type semiconducting behavior, the ESR change from paramagnetic to ferromagnetic resonance at T_C, a big value of ESR linewidth and its temperature dependence in paramagnetic region were established. The electrical studies revealed the negative magnetoresistance, which can be enhanced with increasing magnetic field and decreasing temperature while a detailed thermopower analysis showed the magnon excitations at low temperatures. The spin-phonon coupling is explained within a

framework of the complex model of paramagnetic relaxation processes as the several-stage relaxation process in which the V^{3+} ions, the exchange subsystem and conduction electrons subsystem act as the intermediate reservoirs.

Keywords: magnetoresistance; spin waves; thermoelectric effects; electron spin resonance

1. Introduction

Kanamori [1] predicted that 90° ferromagnetic (FM) superexchange occurs between octahedrally coordinated $3d^3$ ions. For example, in the *p*-type FM semiconductor $CdCr_2Se_4$ with the Curie temperature T_C = 142 K and the Curie-Weiss (CW) temperature θ_{CW} = 190 K the FM superexchange occurs within the Cr sublattice *via* the 90° Cr-Se-Cr σ/π bonding which links a half-filled $t_{2g}(\pi)$ orbital of one of Cr-ions with an empty $e_g(\sigma)$ level on the other Cr [2,3]. In the parent FM $CuCr_2Se_4$ being a *p*-type metallic conductor with T_C = 416 K and θ_{CW} = 436 K [4], the chromium spins are coupled ferromagnetically *via* double exchange interaction involving the electrons jumping between Cr^{3+} and Cr^{4+} ions [5,6]. The X-ray photoelectron spectroscopy and polarized neutron diffraction study for $CuCr_2Se_4$ provided a direct evidence for the presence of monovalent copper atoms with a $3d^{10}$ configuration [7,8]. However, it was not possible to measure in $CuCr_2Se_4$ the magnetic splitting of the Cr 3*s* levels, because these levels overlapped with the Cu 3*p* ones [7]. The second end composition of the

$CuCr_{2-x}V_xSe_4$ system, *i.e* CuV_2Se_4 is not known, yet. In the isostructural $CuCr_{2-x}V_xS_4$ spinel system a rapid decrease of T_C from 267 K for $x = 0.25$ to 8 K for $x = 1.75$ was observed [9]. This fact has been explained by being weaker Cr-S-V superexchange interactions than the original Cr-S-Cr ones as well by a weakening of the nearest neighbor ferromagnetic Cr-S-Cr interactions due to the initial lattice expansion [9].

Recently, numerous efforts have been made to find a correlation between the thermoelectric power and the double exchange and superexchange interactions in the $CdCr_{2-x}Ga_xSe_4$, $Zn_xCu_yCr_zSe_4$, $Cu_xGa_yCr_zSe_4$ and $Cu_xCo_yCr_zSe_4$ spinel series [10-14]. These studies have shown that the strong ferromagnetic coupling connected mainly with the double-exchange mechanism, makes easier both the magnon excitations and a transfer of the phonon momentum to the electron gas. The opposite behavior for the ferrimagnetic and antiferromagnetic spin arrangements was observed.

It seems thus natural to expect a coupling between the magnon and electron systems leading to the negative magnetoresistance effect in single-crystalline $CuCr_{1.6}V_{0.4}Se_4$ spinel. For that the Bloembergen and Wang model of paramagnetic relaxation processes [15], the high-temperature expansion of the magnetic susceptibility and the thermoelectric power analysis were used.

2. Experiment

2.1. Preparation

The single crystal of $CuCr_{1.6}V_{0.4}Se_4$ spinel was obtained by the chemical

vapour transport method [16] in a closed quartz ampoule containing binary selenide CuSe, and stoichiometric amounts of high purity (99.99%) elements: vanadium and selenium. Anhydrous chromium chloride $CrCl_3$ was used as the chemical transport agent. The ampoule was heated in a horizontal zone furnace for four weeks. The temperature of the solution and crystallization zone was 1273 K and 1223 K, respectively. The resulting single crystal was of octahedral shape with regular {111} faces, the edge length being 4 mm.

For the crystal structure characterization, describing the cation distribution over the tetrahedral and octahedral sites formed by the selenium sublattice, a good quality sample was selected for the intensity data collection with a single crystal X-ray diffraction technique. The intensities were measured with a KM-4/CCD (Oxford Diffraction) instrument, operating in κ geometry and using graphite monochromated MoKα radiation (λ=0.71073 Å). The ω-scan technique was used for data collection. Integration of the intensity data and corrections for Lorentz – polarization effects and absorption were made using *CrysAlis* software [17]. The absorption correction was applied with the Gaussian face-indexed numerical routine [18]. The structure calculations were performed using the SHELXL-97 program system [18].

The chemical composition of the $CuCr_{1.6}V_{0.4}Se_4$ single crystal was determined by the energy-dispersive X-ray spectrometry (EDXRF). The sample was excited by the air-cooled side-window Rh target X-ray tube of 125 μm thickness Be window and ca. 100 μm nominal focal spot size (XTF 5011/75, Oxford Instruments, USA). The X-ray tube was supplied with the XLG high-

voltage generator (Spellman, USA). The tungsten pinhole collimator was used to reduce the size of analyzed area. For the collimators of the size holes of 100, 200, 400, 1000 and 2000 μm, the following focal spot sizes are obtained: 169, 280, 581, 1469, 2888 μm. The X-ray spectra of the samples were collected by thermoelectrically cooled Si-PIN detector (XR-100CR Amptek, Bedford, MA, USA) of 6 mm^2 active area, 500 μm crystal thickness and 12.5 μm Be window thickness. The Si-PIN detector cooled to the temperature of ca. -55°C reaches the resolution of 145 eV at 5.9 keV. The Si-PIN detector was coupled to a multichannel analyzer (PX4 Amptek, Bedford, MA, USA). In the constructed spectrometer, the incidence and take-off angles were 45°. The position of the sample was moved using the X-Y stage and was monitored by CCD camera and two laser pointers. The weight composition of the single crystal under study is as follows: Cu – 13.1 ± 0.2, Cr – 17.3 ± 0.3, V – 4.26 ± 0.08, Se – 65.4 ± 0.8. These values have been converted into percent of the atomic content.

2.2. Electrical and magnetic measurements

The mass magnetization was measured at 4.6 K and in external magnetic fields up to 60 kOe while the static (dc) mass susceptibility measurements were performed in the temperature range 4.2-350 K and in applied external magnetic field of 900 Oe using a Faraday type Cahn RG automatic electrobalance.

The electrical measurements have been done in the temperature range 7-300 K. The electrical resistivity ρ has been measured with the 4-point dc method using the apparatus with Keithley K181 digital multimeters. The maximal error

$\delta\rho/\rho$ was less than ±1 %. The magnetoresistance measurements were performed in the magnetic fields up to 8 T at 4.3, 10, 15, 20 and 40 K and at fixed magnetic field 8 T in the temperature range 7-110 K. The direction of magnetic field was perpendicular to the current sample. The thermoelectric power was measured with a differential method using the temperature gradient ΔT of about 2 K. The accuracy of the value of thermopower was estimated to be better than 3 μV/K. The electrical and thermal contacts between the single crystal and the copper rods were maintained with a silver lacquer mixture (Degussa Leitsilber 200). The thermoelectric power and the electrical resistivity of the same sample were measured along the <001> direction. The crystal orientation about the <001> crystallographic zone axis, was based on 12-18 centered X-ray diffraction reflections with the Bragg angles in the range $107 \leq 2\theta \leq 144°$ (MoKα radiation). The checking electrical measurements in the <111> direction, performed for comparison, showed unimportant difference with those along <001>.

2.3. ESR measurements

The electron spin resonance (ESR) spectra were measured in the temperature range 77-275 K using a 100-kHz field-modulated spectrometer operated at 9 GHz, so that the derivatives of the absorption signals were recorded. A continuous nitrogen flow cryostat was used to study temperature dependence. For ESR measurements the obtained crystals were crushed into powder and diluted in the paraffin to reduce the skin effect. The shape and area

of the ESR spectra were analyzed by numerical method.

3. Results

3.1. Crystallographic properties

Crystal data, experimental details and structure refinement results for the single-crystal of $CuCr_{1.6}V_{0.4}Se_4$ spinel are collected in Table 1. They are showing that the compound crystallizes in a cubic structure with space group $Fd\bar{3}m$ (#227) and the unit cell of dimension a = 1034.99(12) pm, being slightly elongated in comparison with a = 1033.5(3) pm of the parent $CuCr_2Se_4$ [6]. The structure model with the diamagnetic Cu ions occupying the tetrahedral 8*a* positions and the magnetic Cr and V-ions sharing the octahedral 16*d* sites, converged satisfactorily. The site occupancy factors treated as free variables in the least-squares structure refinement, confirmed the sample composition and the cation distribution according to the spinel formula: $Cu[Cr_{1.6}V_{0.4}]Se_4$.

3.2. Electrical and magnetic properties

The electrical resistivity ρ(T) and thermoelectric power S(T) measurements depicted in Fig. 1 reveal a *p*-type semiconducting behaviour of the $CuCr_{1.6}V_{0.4}Se_4$ single crystal. The values of ρ(T) and S(T) are close to those for $CuCr_2Se_4$ [19]. The variation of ρ(T) does not follow a simple exponential behaviour, because a gradual decrease of resistivity and strong slope at T_C with increasing temperature are observed. The S(T) shows a broad hump at 100 K and reaches a minimum at T_C from one side and goes to (0, 0) from the other.

The ρ(T) dependence decreases with increasing magnetic field, revealing the negative magnetoresistance effect shown in Fig. 2. Moreover, the lower temperature, the larger negative magnetoresistance, $\Delta\rho/\rho_0$(H). However, in the temperature range 10-20 K the negative values of $\Delta\rho/\rho_0$(H) increase insignificantly as temperature decreases (Fig. 2).

The results of the magnetic measurements are depicted in Figs. 3 and 4. The dc mass susceptibility vs. temperature, χ_σ(T), shows a ferromagnetic order with the Curie temperature T_C = 193.2 K. Above 200 K, χ_σ^{-1}(T) follows the CW behavior with a positive CW temperature θ_{CW} = 207 K and an effective moment $\mu_{eff} = 2.83\sqrt{MC_\sigma}$ = 5.85 μ_B/f.u., where the molar mass $M \approx$ 482.96 g/mol and the Curie constant $C_\sigma = 8.873\cdot10^{-3}$ K·cm^3/g. This value is somewhat higher than the spin-only value of 5.22 μ_B/f.u. for $3d^3$ Cr^{3+} and $3d^2$ V^{3+} ions as well as of 5.50 μ_B/f.u. for $3d^9$ Cu^{2+}, $3d^3$ Cr^{3+} and $3d^2$ V^{3+} ions. It means that the chromium ions may form a mixed valence band. In Fig. 4 a shape of magnetic isotherm, σ(H), measured up to 60 kOe and at 4.6 K exhibits a saturation magnetization of 53.84 Oe·cm^3/g (4.66 μ_B) at 4 kOe already. In the inset of Fig. 4 a linear increase of magnetization with increasing magnetic field, indicates a lack of spontaneous magnetization below 4 kOe.

3.3. ESR spectra

The resonance spectra for $CuCr_{1.6}V_{0.4}Se_4$ consist of a single line in the range from room temperature to T_1 = 200 K. At room temperature the intensity

of the resonance line is very weak. Below T_1 the spectra were simulated with two profiles. The Figures 5(a), (b) and (c) show the temperature dependence of the ESR parameters: ΔB - linewidth, B_r – resonance field and DI – intensity of the spectrum. The corresponding values of the ΔB and B_r were obtained as the fitting parameters and the DI values were calculated as double integration of the spectrum. Starting from the T = 272 K (ΔB = 159.2 mT) the linewidth values rapidly decrease as the temperature is lowered to T_1 where ΔB = 27.8 mT. Next, the linewidth passes through a minimum and with decreasing temperature shows a continuous broadening. The line-shape analysis shows that the ESR line remains Lorentzian down to T = 212 K, and below this temperature a deviation towards an asymmetrical line occurs. The shift of the resonance field (B_r) from the high temperature value is observed below T = 212 K. In the temperature range from T = 193 K to T = 85 K this effect is very significant. In Fig. 5(c) the temperature evolution of the intensity of the ESR spectrum is shown with the values reduced to T = 272 K. In the temperature range from T = 225 K to T = 183 K, the intensity rapidly increases. The intensity of ESR spectrum defined as DI (double integration of the spectrum) should be proportional to the spin susceptibility of the sample. The Curie temperature estimated from the DI(T) dependence equals 193.8 K. The agreement with the susceptibility measurements is satisfactory thus the ESR data appear to be consistent with the magnetic ones.

4. Discussion

An explanation of the negative magnetoresistance effect in single-crystalline $CuCr_{1.6}V_{0.4}Se_4$ spinel is considered within a framework of spin-spin and spin-phonon couplings and also as a coupling between magnon and electron systems. For that a complex model of the paramagnetic relaxation processes and the thermoelectric power analysis are discussed in detail.

4.1. ESR studies

The linewidth value of $CuCr_{1.6}V_{0.4}Se_4$ at room temperature is about 200 mT. To understand the origin of the observed linewidth we have to estimate the relaxation contributions of the relevant spin-spin and spin-phonon interactions. In the chromium spinels, the Cr^{3+} ions always occupy the B-site of the spinel structure. The local symmetry at the octahedral site leads to the nondegenerate orbital ground state with $S = 3/2$. On the other hand, for the $3d^2$ configuration of V^{3+} ($S = 1$), the ^3F free ion ground state is split by the octahedral field leaving an orbital triplet (T_2) lowest. Because of that, Cr^{3+} is the ion weakly coupled to the lattice in comparison with the fast-relaxing V^{3+} ions [19].

The ESR linewidth, ΔB, is related to the relaxation of the spin system. For individual spins $\Delta B \sim 1/\tau$, where τ is the spin relaxation time. In a dense magnetic material, this relationship is modified since the magnetization relaxes towards an effective field instead of the external field. In the examined compound it can be expected that the presence of V^{3+} ions essentially changes the resonance linewidth. In paramagnetic state (PM) (*i.e.* for $T > 212$ K) the

linewidth can be described by the following expression:

$$\Delta B = \Delta B_{ss} + \Delta B_{s\text{-}ph} \quad (1)$$

where ΔB_{ss} is described by the exchange narrowing theory [20]:

$$\Delta B_{ss} = [(\Delta B_{dd})^2] / B_{ex}, \quad (2)$$

(*i.e.* is proportional to the square of the dipolar produced linewidth ΔB_{dd} divided by the rate of exchange B_{ex}) and $\Delta B_{s\text{-}ph}$ represents the contributions of the spin-phonon interaction.

The complex model of paramagnetic relaxation processes, illustrated in Fig. 6, can be derived by analogy with the model of Bloembergen and Wang [15,21]. The Zeeman subsystem contains Cr^{3+} and V^{3+} ions and the vanadium is directly coupled to the lattice. The exchange subsystem includes the exchange-coupled Cr-Cr, Cr-V, V-V pairs. In the parent $CuCr_2Se_4$ spinel, which is a well studied metallic ferromagnet with T_C = 416 K [4], the high value of T_C is related to the exchange through the current of the hole carriers [5,6] including also the subsystem of conduction electrons. That model explains also a big ESR linewidth for $CuCr_{1.6}V_{0.4}Se_4$ and its temperature dependence in the PM state (Fig. 5(a)). The parameter of the thermal broadening linewidth $b = d(\Delta B)/dT$ = 1.9mT/K is rather high and means a fast energy flow from the spin subsystem to the $CuCr_{1.6}V_{0.4}Se_4$ lattice [22]. We suppose that the process of spin-lattice

relaxation includes both the interaction between the conduction electron spins and magnetic spins (Korringa effect) and also the vibrational modulation of exchange interactions. According to the Huber's and Seehra's theory for magnetically concentrated systems [23,24], the relationship between temperature and resonance linewidth can be explained by the Korringa mechanism [22] and spin-phonon relaxation processes in which are participating broad bands of phonons.

The temperature dependence of ΔB and B_r in the temperature range 212 – 193 K (Fig. 5(a) and (b)) indicates that the magnetic short-range order develops. In this case, the spin correlations act as an effective internal field and therefore cause a shift of the resonance field B_r from that at high temperatures, where no magnetic short-range order exists. Simultaneously, the linewidth ΔB as $T \rightarrow T_C$ from the high temperature side can be written as follows:

$$\Delta B = \Delta B_{noncrit}(T) + \Delta B_{crit}(T), \quad (3)$$

where: $\Delta B_{noncrit}$ and ΔB_{crit} factors represent the noncritical and critical contributions to the linewidth, respectively, and $\Delta B_{noncrit}$ is given by Eq. (1). The growth of linewidth (ΔB_{crit}) reflects the increase in the lifetime and the correlation length of the critical fluctuations. The appearance of the short-range magnetic ordering is confirmed by the temperature dependence of the spectrum intensity (Fig. 5(c)). As the temperature is reduced from about T = 225 K, the values for intensity rapidly increase. The ferromagnetic ordering temperature T_C

= 193.8 K can be inferred from the location of coincident anomalies in the ESR data: ΔB, B_r, DI (Fig. 5). The ESR spectrum of $CuCr_{1.6}V_{0.4}Se_4$ observed below T = 193 K undergoes qualitative changes and transforms from paramagnetic (EPR) into ferromagnetic (FMR) resonance. At low temperatures the experimental spectrum was fitted by two profiles shown in Fig. 5(a) and (b). It is known, that FMR can be adequately described in terms of the Landau-Lifshitz-Gilbert equation [25] for the effective internal magnetic fields, which are attributed to demagnetization and magnetocrystalline anisotropy fields. However, as in our resonance measurements the sample in powdered form was examined, the shape of FMR spectrum is the envelop of several components. As can be seen from Fig. 5(a) and (b), the position and linewidth of this spectrum depends monotonously on the temperature.

4.2. Thermoelectric power analysis

In this section we consider a coupling between the magnon and electron systems based on the thermoelectric power analysis. Generally, in the magnetic materials the magnetic component of thermopower (MCTP) may result from a coupling of the phonon system to the electron gas via the spin lattice (magnon gas), which is known as the Kasuya model [26], or from the transfer of the magnon momentum to the electron gas (magnon drag) [27]. This magnetic contribution is described by the Bloch law [28], *i.e.* the spontaneous magnetization decreases with temperature at $T^{3/2}$ when T is small [29]. Analogous temperature dependence of MCTP has been directly derived from a

theoretical model of magnon-assisted transport in a mesoscopic tunnel junction between a ferromagnetic metal and a normal (nonmagnetic) metal [30] for a magnetic component of thermoelectric power.

The experimental curve shape of thermopower *S(T)* of the spinel single crystal under study (Fig. 1) can be easily fitted by the modified Matoba, Anzai and Fujimori semiempirical formula [31] including the magnetic contribution [13] as follows:

$$S(T) = D \cdot T + E \cdot T^3 + \frac{F \cdot (\frac{T}{\theta_D})^3}{G + (\frac{T}{\theta_D})^4} + H \cdot T^{1/2} + \frac{I \cdot (\frac{T}{J_{eff}^{aa}})^{3/2}}{K + (\frac{T}{J_{eff}^{aa}})^{5/2}} \qquad (4)$$

where θ_D is the Debye temperature (see Appendix A), and J_{eff}^{aa} is the effective exchange integral for the first coordination sphere (see Appendix B). First and second terms in Eq. (4) is the diffusion component where the small correction *E* is the temperature dependence of *D* [32], third term in Eq. (4) is the phonon drag component, fourth term in Eq. (4) is the impurity component, and the last term in Eq. (4) is the magnon drag component. *D, E, F, G, H, I* and *K* in Eq. (4) (listed in Table II) are the curve-fitting parameters. The agreement index *R* between the experimental (S_{exp}) and the theoretical (S_{theor}) thermopowers is high (over 99 %, see Table 2).

The results of thermopower analysis of the single-crystalline $CuCr_{1.6}V_{0.4}Se_4$ depicted in Fig. 7 show that the intensity of the magnon drag component (S_{mag}) is the largest and reaches a maximum of 7.86 μV/K at 33 K. It means that the magnon excitations, usually driven by the double exchange mechanism, are observed only at low temperatures, and the maximum transfer of the magnon

momentum to the electron gas may be a main reason for the observed the negative magnetoresistance effect. This effect disappears at higher temperatures. The contribution to the total thermopower originates then mainly from the phonon component (S_{ph}) which reveals a maximum of 7.1 μV/K at 100 K, *i.e.* exactly in the theoretical temperature range $\theta_D/10 - \theta_D/2$ predicted by the Debye theory [27], where in our case θ_D = 279.7 K (see Table 2). At high temperatures the diffusion component (S_{diff}) dominates, and according to the Mott formula [33] it is proportional to temperature. The S_{diff} = 5.6 μV/K at 300 K. The so-called impurity component of the thermopower (S_{imp}) described by the $T^{1/2}$ law [34] generates a maximum 1.51 μV/K at 300 K.

From the results of the magnetic considerations presented in Table 3 (see Appendix B) it follows that with increasing vanadium content x: (1) contribution of the superexchange interaction to the Curie-Weiss temperature θ_{CW} suddenly increases from 90 K for $CuCr_2Se_4$ to 163 K for $CuCr_{1.6}V_{0.4}Se_4$, (2) contribution of the double exchange interaction to the Curie-Weiss temperature θ_{CW} and the total hopping integral B rapidly decrease, and (3) the W_d bandwidth of the $3d$ t_{2g} band due to Cr^{3+} and Cr^{4+} ions decreases from 0.76 eV for $CuCr_2Se_4$ to 0.11 eV for $CuCr_{1.6}V_{0.4}Se_4$. In the studied single crystal the superexchange J_{aa} and J_{ab} integrals for the first two coordination spheres are positive and negative, respectively, the absolute value of J_{aa} is over nine times larger than J_{ab}, the double exchange b_{aa} and b_{ab} integrals for the first two coordination spheres are positive and b_{aa} is five times larger than b_{ab}, and the effective exchange

constants J_{eff}^{aa} and J_{eff}^{ab} for the first two coordination spheres are positive and negative, respectively, and the absolute value of J_{eff}^{aa} is more than five times larger than J_{eff}^{ab}. The calculated magnetic parameters above mentioned well correlate with semiconducting properties and strongly reduced both the long and short range FM interactions of the $CuCr_{1.6}V_{0.4}Se_4$ spinel. For comparison, the relevant calculated magnetic parameters [13] of the parent $CuCr_2Se_4$ metallic ferromagnet [5] are collected in Table 3.

5. Conclusions

We have shown that in ferromagnetic semiconductor $CuCr_{1.6}V_{0.4}Se_4$, exhibiting high electrical conductivity the magnon excitations are connected with a double exchange mechanism existing apart from the superexchange interaction, like it was observed in the ferromagnetic spinel systems: $Zn_xCu_yCr_zSe_4$ for $y \geq 0.8$ [11], $Cu_xGa_yCr_zSe_4$ for $0.036 \leq y \leq 0.394$ [12], $Cu_xCo_yCr_zSe_4$ for $0.06 \leq y \leq 0.11$ [13], and indicated by de Gennes in manganites [35]. For comparison, in the $CdCr_{2-x}Ga_xSe_4$ spinel system [10], the ferromagnetic coupling, being caused only by the superexchange mechanism, does not contribute to the spin wave excitations. The big value of ESR linewidth of $CuCr_{1.6}V_{0.4}Se_4$ and its strong temperature increase in PM state suggest the weakly exchange-coupled Cr-Cr pairs to the lattice in comparison with the fast-relaxing V^{3+} ions. The spin-phonon coupling is explained as the several-stage relaxation process in which the V^{3+} ions, the exchange subsystem and

conduction electrons subsystem act as the intermediate reservoirs.

Our results mean that in the mixed Cr valence band with a narrow bandwidth of 0.11 eV a coherent transfer of the magnon momentum to the electron gas results in the negative magnetoresistance effect in the single crystal under study.

Acknowledgments

This work was partly supported by Ministry of Science (Poland) and funded from science resources for years 2007-2009 as a research project (Project No. N N204 178433). We are indebted to the European Community for the UPGOW fellowship awarded to S. Mazur for the year 2008-09.

Appendix A

The Debye temperature [36], θ_D, has been estimated from the following formula:

$$\theta_D = \frac{hv}{2k}\sqrt[3]{\frac{6\pi^2 N}{V}} \qquad \text{(A1)}$$

where h is the Planck constant, k is the Boltzmann constant, N = 56 is the number of atoms in the spinel unit cell, V (= a^3, where a is the lattice parameter) is the volume of the spinel unit cell and v = 809 m/s is the sound speed in the $CuCr_2Se_4$ spinel calculated from Eq. (A1) and based on the value of θ_D = 280 K estimated from the heat capacity measurements and the Grüneisen constant.[37] We assumed the same value of the sound speed in the $CuCr_{1.6}V_{0.4}Se_4$ spinel and

the calculated value of θ_D for this spinel is of the same order as for the $CuCr_2Se_4$ one (see Table 2).

Appendix B

To determine the exchange constants of the superexchange and double exchange interactions an estimation of the Cr^{3+} and Cr^{4+} portions is necessary. Portions x_3 and x_4 of the chromium ions: Cr^{3+} and Cr^{4+}, respectively, were calculated from the saturation magnetization M_s:

$$M_s = 2(g_3S_3x_3 + g_4S_4x_4 + g_4S_4x) \quad \text{(B1)}$$

taking into account the following normalization condition: $x_3 + x_4 + x = 1$, where $M_s = 4.66\ \mu_B$ is the experimental value of the saturation magnetization, $S_3 = 3/2$ is the spin of Cr^{3+} ion, $S_4 = 1$ is the spin of Cr^{4+} and V^{3+} ions, $g_3 = 2.0$ and $g_4 = 1.86$ are the Landé factors for Cr^{3+}, Cr^{4+} and V^{3+} ions, respectively, and $x = 0.2$ is the normalized content of V^{3+} ions.

The exchange constants of superexchange and double exchange interactions between the first two coordination spheres were calculated using the exchange Hamiltonian as follows:

$$H = H_{se} + H_{de} \quad \text{(B2)}$$

where:

$$H_{se} = -\sum_{\substack{i,j \\ i \neq j}} J_{ij} \vec{S}_i \cdot \vec{S}_j , \quad \text{(B3)}$$

represents the superexchange Cr^{n+}-Se-Cr^{m+} and Cr^{m+}-Se-Se-Cr^{n+} interactions [4] with the integrals J_{ij} and $c_{aa} = 6$ and $c_{ab} = 12$ numbers of nearest neighbours in

the first and second Cr-Cr coordination spheres, respectively. The spins $\vec{S}_i$ and $\vec{S}_j$ are considered as the quasiclassical vectors.

$$H_{de} = -\tfrac{1}{6} x_3 x_4 \sum_{\substack{i,j \\ i \neq j}} b_{ij} \vec{S}_i \cdot \vec{S}_j \,, \qquad \text{(B4)}$$

represents the double exchange interactions [4] with x_3 and x_4 being the concentration of Cr^{3+} and Cr^{4+} ions, which is normalized in such way that $x_3 + x_4 + x = 1$ as from the ESR studies it follows that V^{3+} ions are directly coupled to the lattice, and b_{ij} is the hopping integral between the atomic t_{2g} states $|i\rangle$ and $|j\rangle$ for neighbours $\langle i,j\rangle$. We take the band factor as $\sim x_3 x_4$ corresponding to probability of finding one atom in the state Cr^{3+} and the neighbouring one in the state Cr^{4+}. The number 1/6 in the double exchange Hamiltonian (B4) is a constant of a bilinear term $\vec{S}_i \cdot \vec{S}_j$ in the case of spin 1 [38]. Additionally, we take the hopping electron between two Cr ions on the same footing as the remaining ones. Because all t_{2g} electrons are quantum mechanically indistinguishable, the Cr cations supply both localized and itinerant 3*d* moments when Cr^{4+} cations are present [4].

According to the Hamiltonian (B2) the effective exchange constants [4] for the first two coordination spheres are:

$$J_{eff}^{aa} = J_{aa} c_{aa} + \tfrac{1}{6} b_{aa} c_{aa} x_3 x_4 \,, \qquad \text{(B5)}$$

$$J_{eff}^{ab} = J_{ab} c_{ab} + \tfrac{1}{6} b_{ab} c_{ab} x_3 x_4 \,. \qquad \text{(B6)}$$

The J_{aa} and b_{aa} and J_{ab} and b_{ab} integrals for the first two coordination spheres, respectively, are calculated from the high temperature expansion of the magnetic susceptibility [4]. These calculations are based on the equations describing the

contributions to the paramagnetic Curie-Weiss temperature resulting from the separate mechanisms of the superexchange and double exchange interactions as follows [39]:

$$\theta_{CW} = \theta_{se} + \theta_{de} \quad \text{(B7)}$$

where θ_{CW} is the paramagnetic Curie-Weiss temperature (from experiment), θ_{se} is the superexchange contribution to θ_{CW} and θ_{de} is the double exchange contribution to θ_{CW}. The above contributions [4,39] can be read:

$$\theta_{se} = \tfrac{2}{3} X \sum_p J_p c_p \,, \quad \text{(B8)}$$

$$\theta_{de} = \tfrac{1}{6} X x_3 x_4 \sum_p b_p c_p \,, \quad \text{(B9)}$$

where $\sum_p J_p c_p = \theta_{Cu}$ was taken from Ref. 4 and equal to 90 K for the $CuCr_2Se_4$ metallic ferromagnet, which means only the pure superexchange contribution, $B = \sum_p b_p c_p$ is the total hopping integral for the first and second coordination spheres and X is a mixture of spins due to the presence of Cr^{3+}, Cr^{4+} and V^{3+} ions. A summation over p means the summation over the consecutive coordination spheres, each of them containing c_p neighbours of a given central atom. We should set:

$$X = x_3 S_3(S_3 + 1) + x_4 S_4(S_4 + 1) + x S_4(S_4 + 1). \quad \text{(B10)}$$

Finally, Eq. (B7) can be written:

$$\theta_{CW} = \tfrac{2}{3} X \theta_{Cu} + \tfrac{1}{6} X x_3 x_4 B \,, \quad \text{(B11)}$$

with the following superexchange and double exchange contributions to θ_{CW}, respectively:

$$\theta_{se} = \tfrac{2}{3} X\theta_{Cu}\,, \tag{B12}$$

$$\theta_{de} = \tfrac{1}{6} X x_3 x_4 B\,. \tag{B13}$$

Eq. (B11) allows to estimate the mixed valence (Cr^{3+},Cr^{4+}) bandwidth, W_d, of the $3d\ t_{2g}$ band from the relation [4]:

$$W_d = 2B. \tag{B14}$$

Using the Holland and Brown equations [40] we can calculate the superexchange integrals J_{aa} and J_{ab} for the first two coordination spheres, taking into account the estimated values of θ_{se} from Eq. (B12) and the experimental values of the Curie temperature T_C.

$$\theta_{se} = 5(3J_{aa} + 18J_{ab}), \tag{B15}$$

$$T_C = 5(J_{aa} - 2J_{ab}). \tag{B16}$$

The double exchange b_{aa} and b_{ab} integrals[4] can be calculated from the equation:

$$B = 6b_{aa} + 36b_{ab}\,, \tag{B17}$$

where b_{aa} stands for the contribution from the 6 nearest neighbours and b_{ab} stands for the contributions from the 36 second nearest neighbours and from the Lotgering [5] considerations:

$$b_{aa} = 5b_{ab} \tag{B18}$$

The calculated magnetic parameters: θ_{se}, θ_{de}, B, W_d, J_{aa}, J_{ab}, J_{ab}, b_{aa}, b_{ab}, J_{eff}^{aa}, J_{eff}^{ab} are collected in Table 3.

References

[1] J. Kanamori, J. Phys. Chem. Solids 10 (1959) p.87.

[2] P.K. Baltzer, P.J. Wojtowicz, M. Robbins and E. Lopatin, Phys. Rev. 151

(1966) p.367.

[3] P.K. Baltzer, H.W. Lehmann and M. Robbins, Phys. Rev. Lett. 15 (1965) p.493.

[4] J. Krok, J. Spałek, S. Juszczyk and J. Warczewski, Phys. Rev. B 28 (1983) p.6499.

[5] F.K. Lotgering, in *Proceedings of the International Conference on Magnetism, Nottingham*, 1964 (Institute of Physics, London, 1965), p.533.

[6] F.K. Lotgering and R.P. Van Stapele, Solid State Commun. 5 (1967) p.143.

[7] C.Th. Hollander, G. Sawatzky and C. Haas, Solid State Commun. 15 (1974) p.747.

[8] O. Yamashita, Y. Yamaguchi, I. Nakatani, H. Watanabe and K. Masumoto, J. Phys. Soc. Japan 46 (1979) p.1145.

[9] M. Robbins, A. Menth, M.A. Miksovsky and R.C. Sherwood, J. Phys. Chem. Solids 31 (1970) p.423.

[10] T. Groń, A. Krajewski, J. Kusz, E. Malicka, I. Okońska-Kozłowska and A. Waśkowska, Phys. Rev. B 71 (2005) p.035208.

[11] T. Groń, A. Krajewski, H. Duda and P. Urbanowicz, Physica B 373 (2006) p.245.

[12] T. Groń, S. Mazur, H. Duda, J. Krok-Kowalski and E. Malicka, Physica B 391 (2007) p.371.

[13] T. Groń, S. Mazur, H. Duda, J. Krok-Kowalski and E. Maciążek, J. Alloys Compd. 467 (2009) p.112.

[14] S. Mazur, T. Groń and I. Jendrzejewska, J. Alloys Compd. 480 (2009) p.19.

[15] N. Bloembergen and S. Wang, Phys. Rev. 93 (1954) p.72.

[16] I. Okońska-Kozłowska and J. Kopyczok, Acta. Cryst. C49 (1993) p.1448.

[17] *CrysAlis CCD* and *CrysAlis RED*, Oxford Diffraction Ltd., (2004) Wrocław, Poland.

[18] G.M. Sheldrick, "SHELXL-99, Program for the Refinement of Crystal Structures", University of Göttingen, 1997.

[19] C. A. Bates, A. Gavaix, P. Steggles, A. Vasson and A. M. Vasson, J. Phys. C: Solid State Phys. 9 (1976) p.2413.

[20] A. Bencini and D. Gatteshi, *Electron Paramagnetic Resonance of Exchange Coupled Systems*, Springer-Verlag, Berlin Heidelberg, 1990.

[21] A. Abragam and B. Bleaney, *Electron Paramagnetic Resonance of Transition Ions*, Clarendon Press, Oxford, 1970.

[22] S.E. Barnes, Adv. Phys. 30 (1981) p.801.

[23] D.L. Huber and M.S. Seehra, J. Phys. Chem. Solids 36 (1975) p.723.

[24] M.S. Seehra, M.M. Ibrahim, V.S. Babu and G. Srinivasan, J. Phys.: Condens. Matter 8 (1996) p.11283.

[25] S.M. Bhagat and P. Lubitz, Phys. Rev. B 10 (1974) p.179.

[26] T. Kasuya, Progr. Theor. Phys. 22 (1959) p.227.

[27] H.J. Trodahl, Phys. Rev. B 51 (1995) p.6175.

[28] C. Kittel, *Introduction to solid state physics*, John Wiley & Sons Inc., New York, 1966.

[29] J. Callaway, *Quantum theory of the solid state*, Academic Press, New York and London, 1974.

[30] E. McCann and V.I. Fal'ko, J. Mag. Mag. Mater. 268 (2004) p.123.

[31] M. Matoba, S. Anzai and A. Fujimori, J. Phys. Soc. Jpn. 63 (1994) p.1429.

[32] M. Matoba, S. Anzai and A. Fujimori, J. Phys. Soc. Jpn. 60 (1991) p.4230.

[33] F.J. Blatt, P.A. Schroeder, C. Foiles and D. Greig, *Thermoelectric power of metals*, Plenum, New York, 1976.

[34] N.F. Mott, *Conduction in non-crystalline materials*, Oxford Univ. Press, New York, 1987.

[35] P.G. de Gennes, Phys. Rev. 118 (1960) p.141.

[36] P. Debye, Ann. Physik 39 (1912) p.789.

[37] Yu. Tretyakov, I.V. Gordeev and Ya.A. Kesler, J. Solid State Chem. 20 (1977) p.345.

[38] M. Cieplak, Phys. Rev. B 18 (1978) p.3470.

[39] J. Krok-Kowalski and J. Warczewski, J. Mag. Mag. Mater. 83 (1990) p.485.

[40] W.E. Holland and H.A. Brown, Phys. Status Solidi A 10 (1972) p.249.

Table 1. Crystal data, experimental details and structure refinement results for the $CuCr_{1.6}V_{0.4}Se_4$ single crystal.

(I) Crystal data and experimental details

Structural formula	$(Cu)[Cr_{1.6}V_{0.4}]Se_4$
Space group	$Fd\bar{3}m$ (#227)
Lattice parameter a (pm)	1034.99(12)
Z	8
Calculated density d (Mg/m^3)	5.818
Crystal size (mm×mm×mm)	0.13×0.13×0.14
Maximum 2θ (deg)	90.52
Index ranges: h	-13, 20
k	-20, 16
l	-20, 13
Reflections collected	5589
Independent reflections	262
Data/parameters	190/10
Extinction correction	0.0029(2)
Final R indices [I>2 σ(I)]: R_1; wR_2	2.79; 6.55
Goodness of fit on F^2	1.009
Minimum and max $\Delta\rho$ ($eÅ^{-3}$)	-2.57; 2.86

(II) Fractional atomic coordinates and isotropic displacement parameters (10^3×$Å^2$)

Atom	Site	x	y	z	U_{iso}	Occupancy
Cu	8*a*	0.125	0.125	0.125	9.2(1)	1.0
Cr	16*d*	0.5	0.5	0.5	10.4(2)	0.8
V	16*d*	0.5	0.5	0.5	10.4(2)	0.2
Se	32*e*	0.25691(3)	0.25691(3)	0.25691(3)	13.99(2)	1.0

(V) Selected interatomic distances (Å) and bond angles (deg)

Cu – Se (pm)	236.47(5)
Cr/V – Cu (pm)	429.08(5)
Cr – Se (pm)	251.80(3)
Cr – Cr (pm)	365.92(4)
Se – Se shortest (pm)	345.70(8)
Se – Se (pm)	366.20(4)
Se – Cu – Se (deg)	109.47(0)
Se – Cr/V – Se (deg)	93.30(1)
Se – Cr – Se ^{i} (deg)	86.70(1)

Note: The superscript *i* denotes symmetry operator generating equivalent atom at x+1/4, y+1/4, 1-z.

Table 2. The fitting parameters: *D, E, F, G, H, I* and *K* in Eq. (4) of the thermoelectric power analysis of the $CuCr_{1.6}V_{0.4}Se_4$ single crystal.

D ($\mu V/K^2$)	E ($\mu V/K^4$)	F ($\mu V/K$)	G (10^{-3})	H ($\mu V/K^{1.5}$)	I ($\mu V/K$)	K (10^{-3})	R %	θ_D (K)
0.0227	$1.3 \cdot 10^{-15}$	3.473	0.0054	0.0276	2.169	0.0071	99.3	279.7

R is the agreement index. The Debye temperature θ_D has been calculated from Eq. (A1).

Table 3. The calculated magnetic parameters: *X*, θ_{se}, θ_{de}, *B*, W_d, J_{aa}, J_{ab}, b_{aa}, b_{ab}, J_{eff}^{aa} and J_{eff}^{ab} of the $CuCr_{2-2x}V_{2x}Se_4$ spinel system.

x (V^{3+})	x_3 (Cr^{3+})	x_4 (Cr^{4+})	X	θ_{se} (K)	θ_{de} (K)	B (K)	W_d (eV)	J_{aa} (K)	J_{ab} (K)	b_{aa} (K)	b_{ab} (K)	J_{eff}^{aa} (K)	J_{eff}^{ab} (K)
0	0.512	0.488	2.896	90	340	4391	0.76	63.9	-9.65	332.65	65.53	466.51	-83.05
0.2	0.41	0.39	2.718	163	44	607	0.11	31.7	-3.47	45.98	9.2	197.55	-38.7

The values for $x = 0.0$ are taken from Ref. 13 for comparison.

Figure captions:

Figure 1. Electrical resistivity ρ and thermoelectric power S vs. temperature T.

Figure 2. Magnetoresistance $\Delta\rho/\rho_0$ vs. magnetic induction B at 4.3, 10, 15, 20 and 40 K.

Figure 3. Temperature dependences of mass susceptibility χ_σ and reciprocal mass susceptibility χ_σ^{-1} recorded at H = 900 Oe. The Curie temperature T_C = 193.2 K is indicated by arrow.

Figure 4. Mass magnetisation σ vs. magnetic field H at 4.6 K. σ_s = 53.84 Oe·cm^3/g and μ_s = 4.66 μ_B are the saturation magnetisation and saturation magnetic moment, respectively. The saturation state is marked by dashed line. Inset: the onset of the σ(H) dependence up to 1.0 kOe.

Figure 5. The temperature dependence of the ESR parameters: (a) the resonance linewidth ΔB, (b) the resonance field B_r and (c) intensity of the spectrum DI. The Curie temperature T_C = 193.8 K is indicated by arrow and separates FMR and EPR resonances.

Figure 6. Model of paramagnetic relaxation processes of the $CuCr_{1.6}V_{0.4}Se_4$ spinel system.

Figure 7. The thermopower analysis of the $CuCr_{1.6}V_{0.4}Se_4$ spinel where S_{exp} is the experimental curve, S_{theor} is the theoretical curve and S_{diff}, S_{ph}, S_{imp} and S_{mag} are diffusion, phonon drag, impurity and magnon drag components of thermopower, respectively.

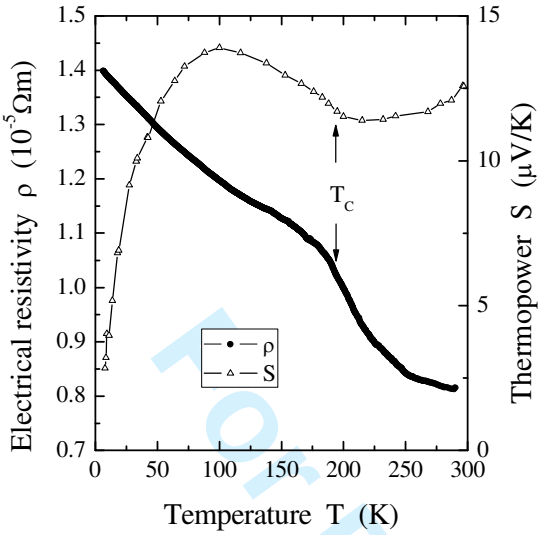

Fig.1

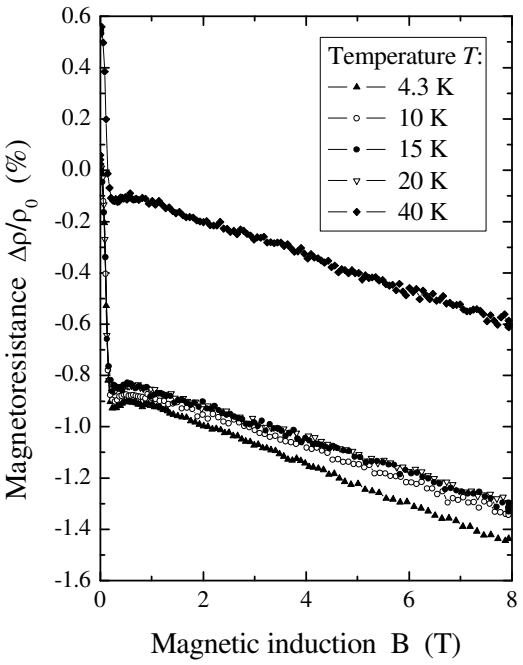

Fig.2

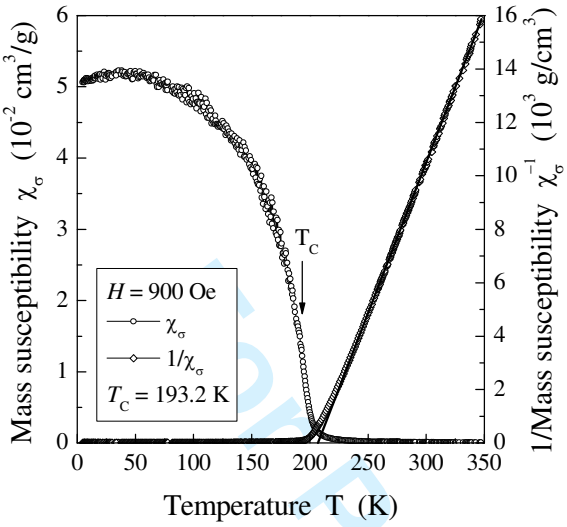

Fig.3

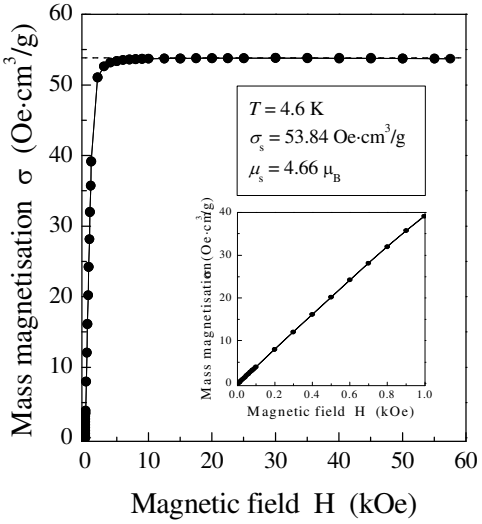

Fig.4

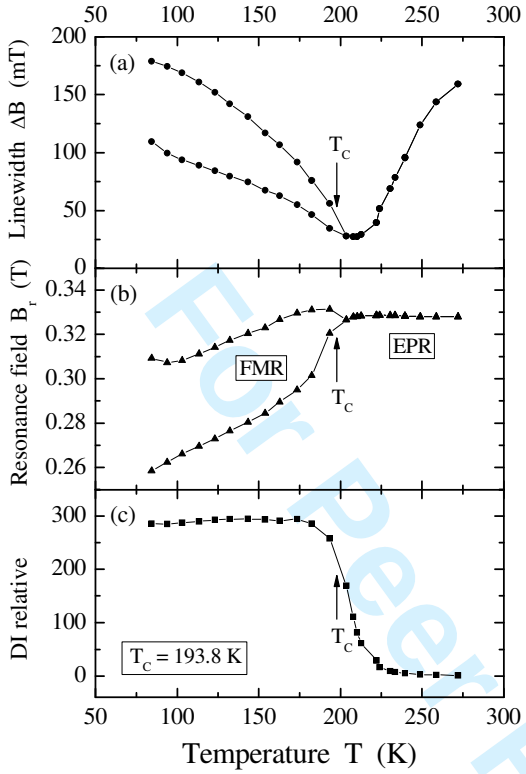

Fig.5

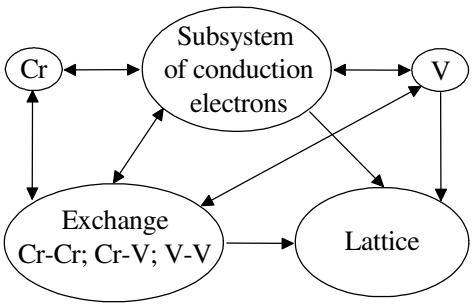

Fig.6

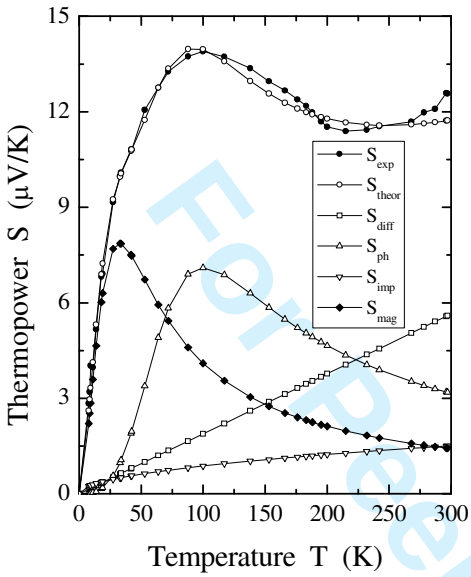

Fig.7